FLIGHT INVESTIGATIONS OF TOLLMIEN-SCHLICHTING WAVES ON AN AIRCRAFT WING

ICAS-90-6.1.2

K.H. Horstmann and G. Redeker

Deutsche Forschungsanstalt für Luft- und Raumfahrt e.V. (DLR
Institut für Entwurfsaerodynamik
D-3300 Braunschweig, Fed. Rep. Germany

S.J. Miley

Aerospace Engineering
Royal Melbourne Institute of Technology
Melbourne, Victoria 3001

Abstract

Hot-wire anemometer measurements have been carried out in flight to investigate, in detail, laminar boundary layer instability on a special wing glove. Tollmien-Schlichting (TS) waves are easily identifiable, and specific measurements of amplitude, frequency and wavelength have been made. The measured values compare well with results from linear stability analysis utilizing the laminar boundary layer calculated from flight measurements of the wing glove pressure distribution. Comparisons between the measured distribution of the velocity fluctuations and the calculated Eigenfunction show some variation. This may be due to nonlinear behavior of the TS waves.

Nomenclature

A_0 initial amplitude of waves in the laminar boundary layer at the instability point

A amplitude of amplified Tollmien-Schlichting waves in the laminar boundary layer

C_p static pressure coefficient on wing glove contour

F frequency of Tollmien-Schlichting waves (s^{-1})

l length of wing glove chord (m)

N amplification exponent or N-factor in linear stability theory [$N=\ln(A/A_0)$] obtained after integration of local amplification rates

Re Reynolds number based on glove chord

Re_T Reynolds number based on length of laminar boundary layer

x streamwise coordinate of wing section (m)

y surface normal coordinate of wing section (m)

U velocity within the boundary layer (m/s)

U_{max} velocity at the outer edge of the boundary layer (m/s)

u' time varying or fluctuating part of boundary layer velocity (m/s)

δ thickness of the boundary layer (m)

δ_1 displacement thickness of the boundary layer (m)

λ/l dimensionless wavelength of Tollmien-Schlichting waves

1. Introduction

A more reliable and sophisticated boundary layer transition prediction procedure, compared to simple empirical methods such as Granville [1] and Michel [2], is the application of the e^N or N-factor method [3-6]. Based on the stability theory of laminar boundary layers [7], this method allows the calculation of amplification rates of disturbances of various wavelengths and frequencies of the so-called Tollmien-Schlichting (TS) waves, as illustrated in Fig. 1. From these amplification rates, the amplification ratio, and accordingly, the amplification exponent N can be determined. If it is assumed that a disturbance has a basic amplitude A_0 when it starts amplifying

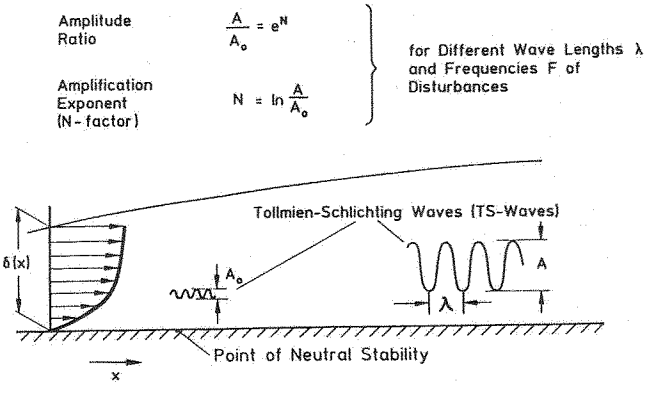

Fig. 1 Instability of laminar boundary layers

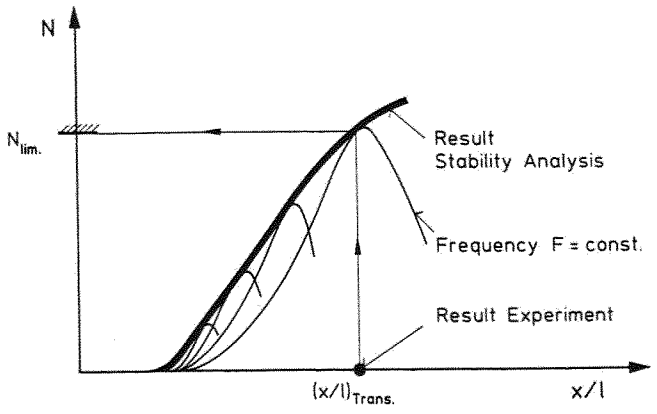

Fig. 2 Transition by means of stability analysis

first, then the amplification ratio A/A_0 at any point can be calculated by integrating the amplification rate up to that point. The amplification ratio can be expressed by an exponential function e^N where N is the amplification exponent or so-called N-factor. It describes the growth of disturbances, which must be evaluated for various wavelengths and frequencies so that N is always a maximum value.

The use of this stability theory for boundary layer transition prediction purposes is demonstrated in Fig. 2. From carefully performed experiments, the maximum calculated N-factor at the experimentally determined transition location has been evaluated and will serve as a limiting N-value in a transition prediction process [8].

The determination of the limiting N-value for flows up to Reynolds numbers $Re = 10^7$ and low Mach numbers has been described in [9]. The data were acquired by means of flight tests on a special laminar flow glove on the DLR LFU-205 experimental aircraft and from wind tunnel tests in DNW. From these investigations, it was concluded that a nearly constant limiting N-value of $N \approx 13.5$ can be assumed for transition prediction. Results of this study are discussed in [9].

In order to base this engineering transition prediction procedure on a more reliable background, a second test phase with the LFU-205 has been carried out. The objective in this phase is to measure the details of laminar boundary layer transition in flight, e.g. Tollmien-Schlichting waves. These measurements will then be compared with calculated results obtained from linear stability theory using the SALLY code of NASA [10].

2. Test Aircraft and Instrumentation

The flight tests were carried out with LFU-205 aircraft of DLR. The LFU-205 is a four-seat experimental aircraft completely built out of glass-fiber reinforced plastics. The general configuration and main dimensions are given in Fig. 3. The maximum level-flight speed is 330 km/h, leading to a Reynolds number based on the aerodynamic mean chord of $Re = 10^7$. The aircraft is equipped with a special laminar glove [9] shown in Fig. 4. It is also made from glass-fiber and contains all flow measurement instrumentation. The static pressure distribution of the glove

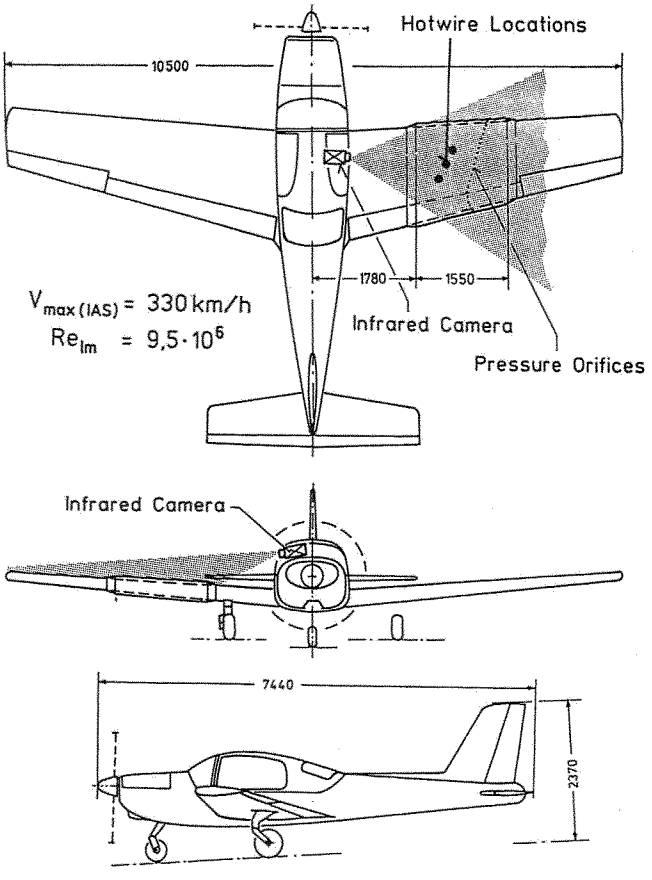

Fig. 3 Flight test aircraft LFU-205

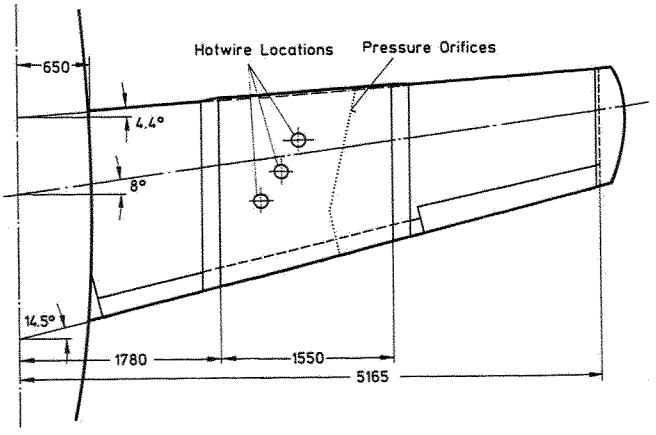

Fig. 4 Laminar glove on LFU-205 wing

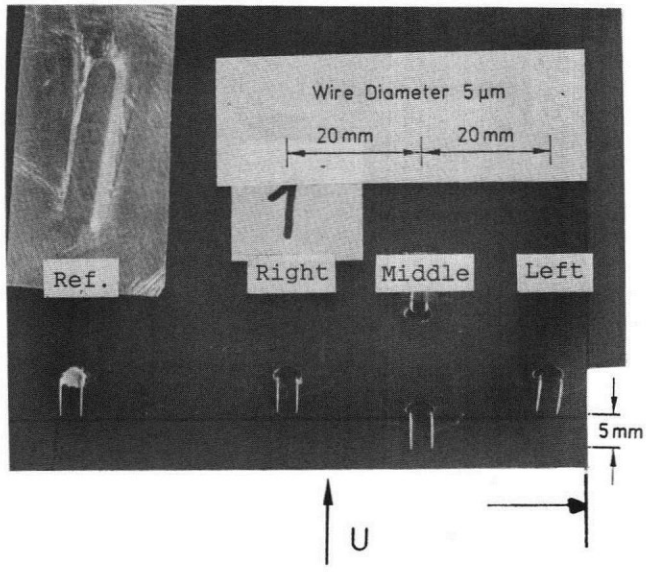

Fig. 5 Hotwire probes on laminar glove

is obtained from 74 pressure orifices arranged in a oblique line relative to the streamwise direction. The details of the pressure sensing and acquisition system are described in [9]. In addition to the pressure instrumentation, the glove is equipped with three hot-wire probe boundary layer traversing systems, located at chord stations x/l = 0.25, 0.43 and 0.58, and also arranged in an oblique line. Each traversing system contains three single-sensor hot-wire probes. Additionally, there is a fourth single-sensor probe mounted separately, adjacent to each of the traversing systems. The probe arrangement is shown in Fig. 5. A cross-sectional view is given in Fig. 6. The three traversing probes, identified as "Left", "Middle" and "Right" are spaced perpendicular to the streamwise direction on 20 millimeter centers, with the "Middle" probe located 5 millimeters forward. The fourth or "Reference" probe is located an additional 40 millimeters laterally on the line through the "Left" and "Right" centers. The purpose of the geometric arrangement of the three traversing probes is to provide a means of determining TS wavelength and wavefront direction through time-correlation of the respective probe signals. The traversing system has a vertical positional accuracy of 10 microns and is operated under computer control. The height of the "Reference" probe is manually adjustable on the ground. The "Reference" probe is used to provide a TS-wave based reference signal with which to normalize the amplitudes measured by the traversing probes at different points in the boundary layer. This normalization is necessary in order to reconstruct the TS-wave amplitude distribution from data taken at different points in time during the traversing operation. All measurements, pressure and hot-wire, including probe traversing, data acquisition, and data storage are under computer software control. A series of programs are available to the flight investigator, to perform different measurement tasks. A detail description of the development and operation of this measurement system is given in [11].

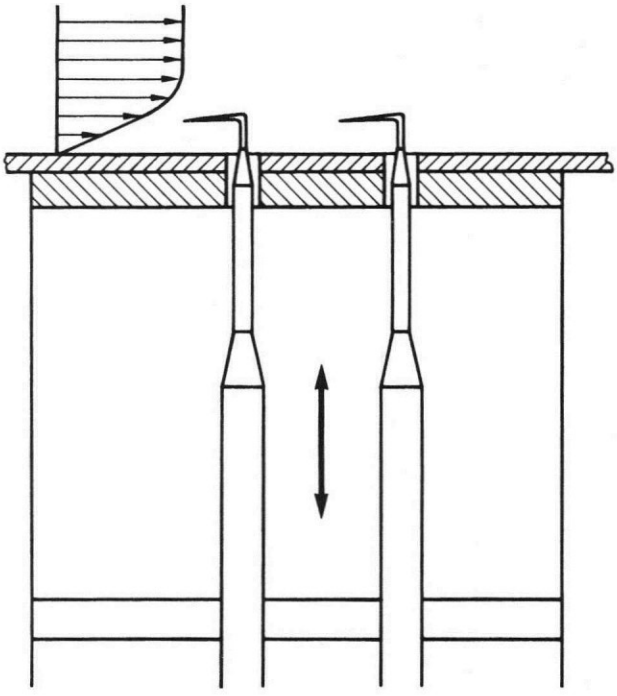

Fig. 6 Cross sectional view of hotwire probe installation

A set of five airspeeds are used to give a range of Reynolds numbers. For a given test airspeed, the chordwise transition point can be adjusted over a range of approximately 30-percent chord through use of the wing flap. The location of the transition point is identified through use

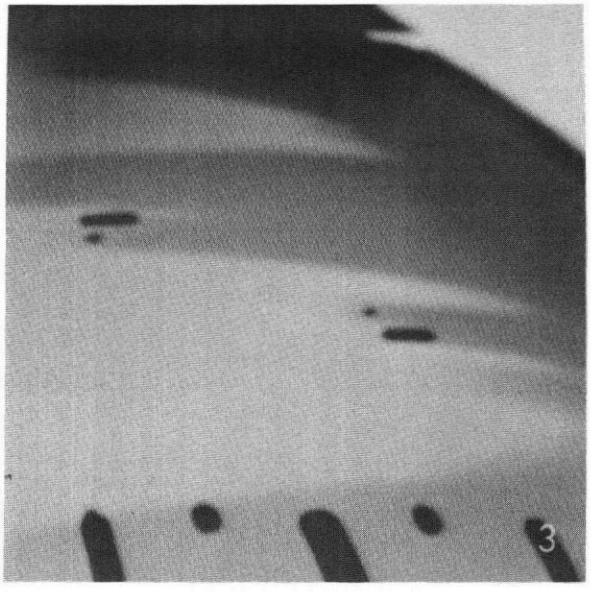

Fig. 7 Infrared image of glove surface in flight

of the infrared image technique [12]. A representative view as seen by the flight investigator is shown in Fig. 7. A typical test point then is obtained by selecting one of the test airspeeds and positioning the transition point relative to the selected hot-wire probe locations using the flap. Glove surface pressure and hot-wire probe data are then taken. The flight investigator can select from four different measurement programs: Hot-Wire Calibration, in which the glove pressure distribution and the flow velocity outside of the boundary layer are measured; TS Profile, in which the glove pressure distribution and up to 40 preselected points within the boundary layer are measured; TS Plot, which provides a real-time plot of the TS-wave amplitude distribution in the boundary layer; and Manual Position, which enables the investigator to position the probes at any point within the boundary layer. Data acquisition time for a 40-point traverse is approximately 150 seconds.

3. Flight Tests and Data Evaluation

The initial flight test results established the validity of the experimental methodology. Tollmien-Schlichting waves were easily identifiable. Frequency-amplitude spectra of the hot-wire signals showed the expected distribution, with frequency increasing with Reynolds number (airspeed). Preliminary estimates of the measured wavelength were within the range of SALLY code predictions. However, a low-frequency large-amplitude signal was also present. This signal was well separated from the TS waves in frequency, however its amplitude was greater than the peak TS wave amplitude, and limited the maximum signal conditioning gains which could be used. This resulted in an unacceptable signal-to-noise ratio. Several flights were used to investigate the source of this low-frequency noise. As discussed in [11], accelerometers had been installed on each of the traversing mechanisms to monitor the vibratory motion of the glove surface. Prior to installation, vibratory modes of the hot-wire probes mounted in the traversing mechanisms had been investigated. No correlation was found between the noise and accelerometer data. As the amplitude of this noise increased towards the surface in the same manner as the TS waves, the possibility of atmospheric turbulence being amplified by the boundary layer was also studies. Again no correlation was found between hot-wire signals outside of the boundary layer and those near the surface. The source of this low-frequency noise was finally traced to a flow interference from the probe access holes in the surface through which the probes were mounted and moved during traversing (see Fig. 6). Fig. 8 shows three different configurations of hot-wire probe access hole, and the corresponding hot-wire anemometer signals. The upper signal associated with the original configuration is representative of the initial flight data. The low-frequency noise was eliminated by filling in the access hole and smoothing the surface as shown in the middle configuration. This configuration however, allowed no traversing motion by the probe. Comparable results were obtained by reducing the access hole diameter to the actual probe support diameter and using a rubber O-ring seal to prevent airflow between the exterior and the interior of the wing.

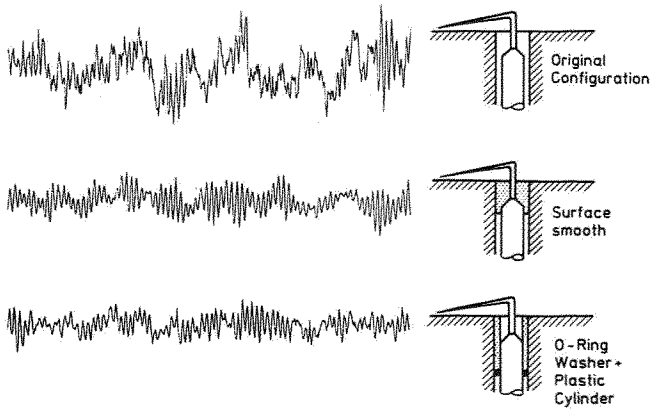

Fig. 8 Influence of probe hole sealing on hotwire signals

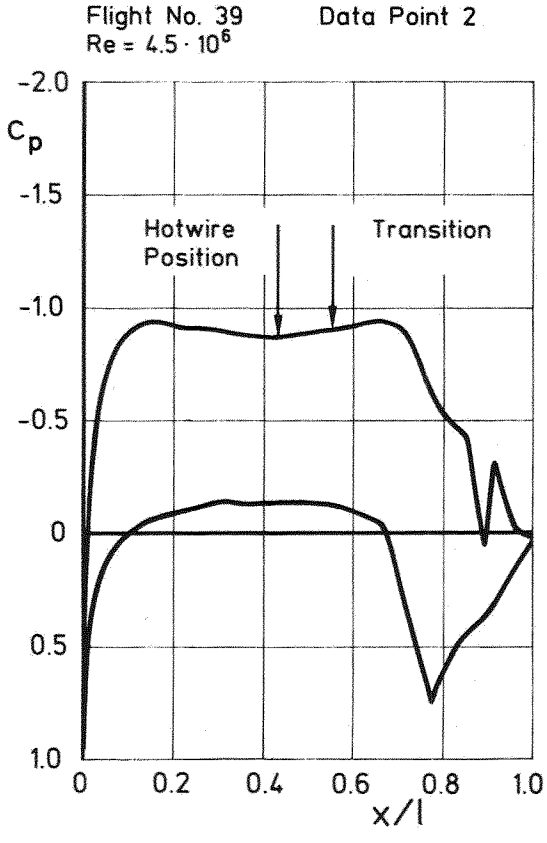

Fig. 9 Flight test pressure distribution on the glove

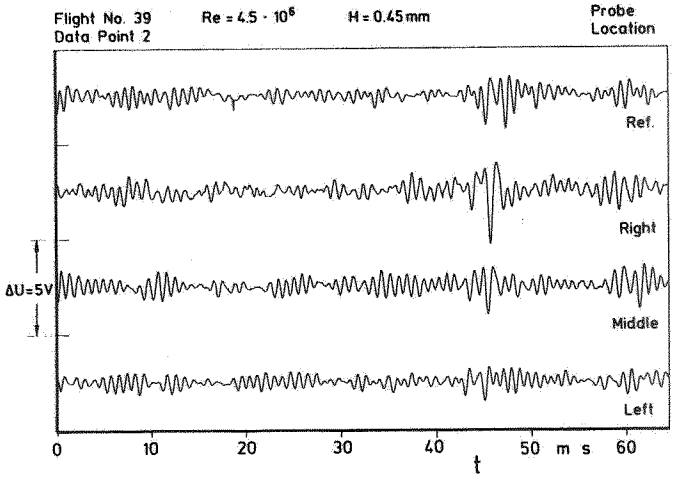

Fig. 10 Time - history of hotwire probe signals

This arrangement, which is the current configuration, is illustrated in the lower part of the figure. The remaining low-frequency modulation of the signal is apparently due to nonlinear behavior of the TS waves, which is is still under study.

Frequency and Wavelength Comparisons

An example of flight test results is given in Fig.'s 9-13. The data point is for a low-speed case. The chordwise pressure distribution is given in Fig. 9. The location of the hot-wire probes and of the transition point are indicated in the figure. From this pressure distribution, the laminar boundary layer is calculated according to [13], and then, amplification factors, frequencies and wavelengths are determined from the SALLY code [10].

A sample of the time-history of the hot-wire probe signals is shown in Fig.10. The data is from the point of maximum TS-wave amplitude in the boundary layer.

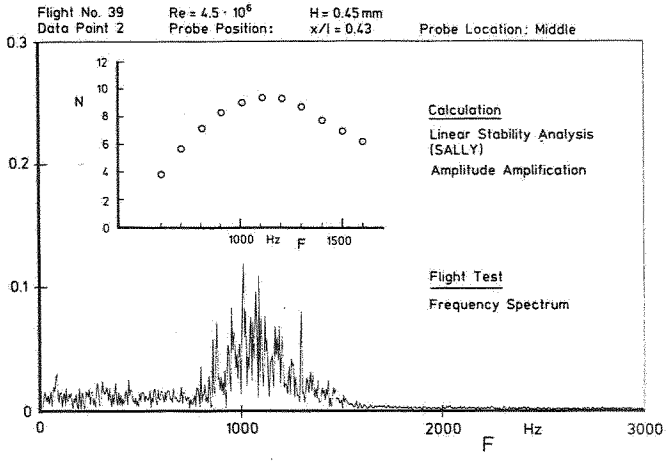

Fig. 11 Measured amplitude-frequency spectrum in comparison with calculated N-factor spectrum

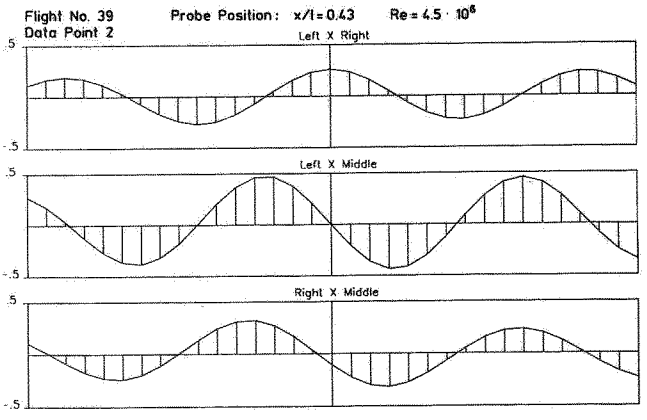

Fig. 12 Cross-correlations of hotwire probe signals

The amplitude-frequency spectrum of the "Middle" probe signal is given in Fig. 11 along with the linear stability analysis prediction. There is good agreement between the predicted amplification factor spectrum and the measured amplitude spectrum. It is noted here that the amplification factor spectrum is based upon the pressure distribution measurement and requires both a boundary layer calculation and a linear stability calculation. Wavelengths from the flight measurement are determined through cross-correlation of the hot-wire probe signals. An example of this is shown in Fig. 12. The respective pairs of probe signals are indicated. The vertical lines denote time-steps (lags) corresponding to the individual data values in the digitized time-history. The wavelength is then determined from the phase angle between a pair of probe signals and the streamwise displacement between the two probes. A comparison between measured and predicted wavelengths is given in Fig. 13. The solid curve is the locus of linear stability solutions corresponding to the streamwise location of the hot-wire probes. The vertical bars mark wavelength values obtained from the

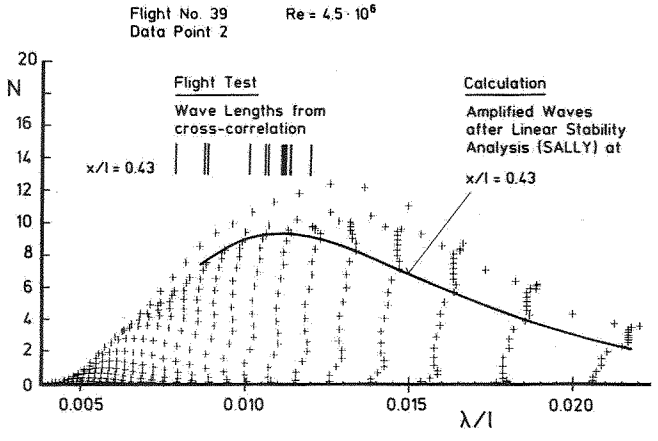

Fig. 13 Measured wavelengths from cross-correlations in comparison with linear stability calculations

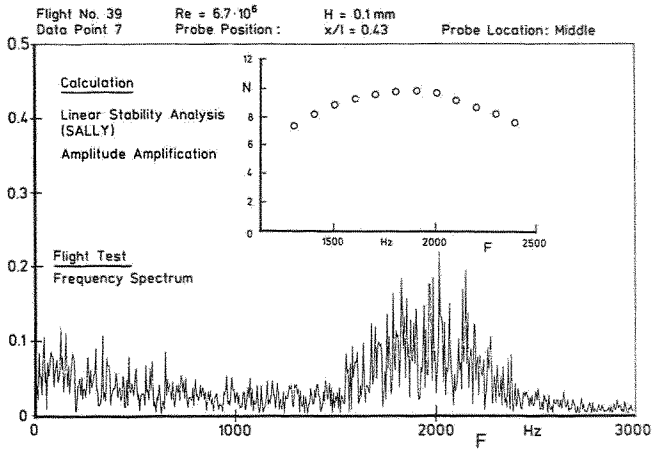

Fig. 14 Measured amplitude-frequency spectrum in comparisons with calculated N-factor spectrum

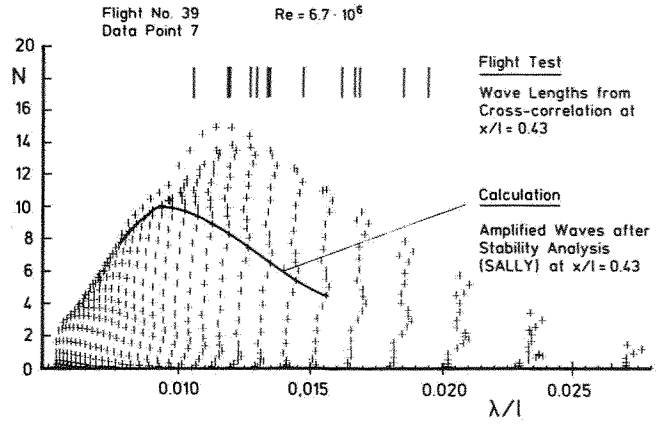

Fig. 15 Measured wavelengths from cross-correlations in comparison with linear stability calculations

probe signals at different traverse points within the boundary layer. The mean of the measured wavelengths lies close to the maximum of the predicted N-factor maximum.

Frequency and wavelength comparisons from a high-speed condition are presented in Fig.'s 14 and 15. Variations between measured data and linear stability predictions are evident here, particularly in regards to wavelength. The mean measured wavelength is well off of the predicted maximum N-factor.

Velocity Profile and Eigenfunction Comparisons

Additional comparisons between theory and flight test are given in Fig.'s 16 and 17. Fig. 16 shows the boundary layer mean velocity profile as calculated from the measured pressure distribution according to [13] and the values from the hot-wire probe. It should be noted here that absolute values from the hot-wire anemometer are dependent on the use of a calibration system which accounts for variations in temperature and sensity between the reference condition on the ground and the flight condition. Fig. 17 presents a comparison between a predicted TS-wave Eigenfunction, according to [14], and the measured TS-wave rms amplitudes within the boundary layer. As the measured amplitudes were taken at different points in time, the amplitude from the "Reference" probe, recorded simultaneously at each data point, was used as a normalizing factor. Considering again, the path by which the predicted results are achieved, the comparison in Fig. 17 is encouraging. The higher vertical position of the measured maximum amplitude is consistent with nonlinear models of instability wave behavior.

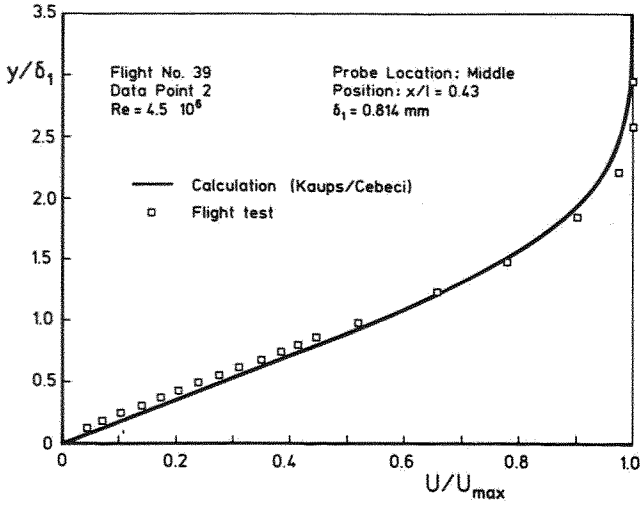

Fig. 16 Measured boundary layer velocity profile in comparison with calculation after Kaups/Cebeci-method

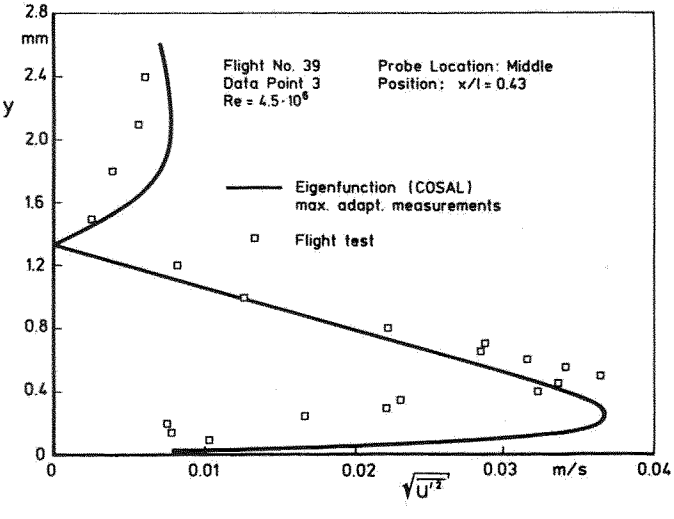

Fig. 17 Measured rms values of fluctuating velocity within the boundary layer in comparison with the calculated Eigenfunction

4. Conclusions

Detail measurements of laminar boundary layer instability have been performed on a wing in flight. Initial comparisons with linear stability theory based upon measured wing pressure distributions are encouraging. Consideration must be given to the disturbance environment which exists on a wing of a propeller driven aircraft. The measurements which have been attempted, have heretofore only been performed on the ground in low turbulence wind tunnels under carefully controlled conditions. Flight measurements represent the real world and it is important to ascertain the validity of current theoretical linear stability models. Some evidence points towards nonlinear behavior of the TS waves. Further analysis of the flight test data is in progress.

References

[1] Granville, P.S.: The calculation of the viscous drag of bodies of revolution.
David Taylor Model Basin Report 849, 1953.

[2] Michel, P.: Critêre de transition et amplification des ondes d'instabilité laminaire.
La Recherche Aerosp. No. 70, 1959, pp. 25-27.

[3] Jaffe, N.A.; Okamura, T.T.; Smith, A.M.O.: Determination of spatial amplification factors and their application to predicting transition.
AIAA Journal, Vol. 8, 1970, pp. 301-308.

[4] Runyan, J.; George-Falvy, D.: Amplification factors at transition on an unswept wing in free flight and on a swept wing in wind tunnel.
AIAA-paper No. 79-0267, 1979.

[5] Hefner, J.N.; Bushnell; D.M.: Status of the linear boundary layer stability theory and the e^N-method with emphasis on swept-wing applications.
NASA TP-1645, 1980.

[6] Obara, C.J.; Holmes, B.J.: Flight-measured laminar boundary layer transition phenomena including stability theory analysis.
NASA TP 3117, 1985.

[7] Schlichting, H.:
Boundary layer theory.
7. Ed. McGraw-Hill, New York, 1979.

[8] Redeker, G.; Horstmann, K.H.: Die Stabilitätsanalyse als Hilfsmittel beim Entwurf von Laminarprofilen.
DGLR Bericht 86-03, 1986, pp. 317-348.

[9] Horstmann, K.H.; Quast, A.; Redeker, G.: Flight and wind-tunnel investigation on boundary layer transition.
J. Aircraft, Vol. 27, 1990, pp. 146-150.

[10] Skrokowski, A.J.; Orszag, S.A.: SALLY level II user's guide.
COSMIC Program No. LAR-12556, 1979.

[11] Miley, S.J.; Horstmann, K.H.; Ketthaus, B.; Krückeberg,C.-P.; Wandert, H.: Direct measurement of laminar instability amplification factors in flight.
DGLR Bericht 88-05, 1988, pp. 93-102.

[12] Quast, A.: Detection of transition by infrared image technique.
ICIASF'87 Record, 1987, pp. 125-133.

[13] Kaups, K.; Cebeci, T.: Compressible laminar boundary layers with suction on swept and tapered wings.
J. Aircraft, Vol. 14, 1977, pp. 661-667.

[14] Malik, M.R.: COSAL - A black box compressible stability analysis code for transition prediction in three-dimensional boundary layers.
NASA CR-165925, 1982.